

# Thermal, structural and morphological assessment of PVP/HA composites

L. C. Mendes · R. C. Rodrigues · E. P. Silva

Received: 18 August 2009 / Accepted: 22 April 2010 / Published online: 7 May 2010  
© Akadémiai Kiadó, Budapest, Hungary 2010

**Abstract** Composites of poly(vinyl pyrrolidone)/hydroxyapatite (PVP/HA), at variable proportions (100/0; 80/20; 50/50; 20/80 wt%) were prepared and characterized by Fourier transformer-infrared spectroscopy (FT-IR), wide angle X-ray diffraction (WAXD), differential scanning calorimetry (DSC), and thermogravimetry/differential thermogravimetry (TG/DTG). PVP carbonyl stretching was slightly shifted to lower frequency in composites indicating the formation of hydrogen bonding with HA hydroxyl groups. At the first cycle of heating, the calorimetric curves revealed a broad peak the intensity of which was reduced insofar as the amount of PVP decreased in the composites. This peak was attributed to the PVP enthalpy relaxation. According to the TG/DTG curves, PVP degraded into two steps sharply perceivable in the composites. The first decay was ascribed to the release of the pyrrolidone pendant groups and the following one concerned the burning of the hydrocarbon chains. The HA molecules seem to exert a catalytic action on the PVP degradation.

**Keywords** PVP · HA · Composite · TG/DTG · FT-IR · WAXD

## Introduction

Naturally occurring phosphate-apatite substances vary in nature and cannot have well tailored properties. This led to researching a synthetic pathway for the production of hydroxyapatite (HA), which would be efficient and simple, and yield a product with controlled structure. The interest in the synthesis of hydroxyapatite (HA) emerged for several reasons. Its use is adequate for many applications, such as water purification, waste stabilization, contaminated soil remediation, heavy metal absorption, and so forth [1]. The loss of bone tissue in humans as a consequence of body injury and/or disease are repaired naturally. However, problems regarding infection resulting from body rejection can arise. The development of synthetic materials with close resemblance to the biological properties of natural bone tissue is required to overcome this problem. Artificially synthesized hydroxyapatite (HA),  $[Ca_{10}(PO_4)_6(OH)_2]$ , has been used as a successful substitute for natural HA, since it is known that the bone tissue of mammals is composed of 58% of calcium hydroxyapatite, a type of calcium phosphate [2–5]. It has been one of the materials of choice for applications such as inorganic scaffolds, bone grafts, etc. in a range of medical and dental applications, due to its interactions with mineral bone components and its osteophilic properties [6–9]. However, its clinical applications have been limited due to low toughness, difficulty in shaping, and its slow degradation rate. With the purpose of overcoming these disadvantages, a number of hybrid materials such as ceramic or polymer composites have been applied as repairing materials to improve biological applications [10–12]. PLGA, PLA and chitosan, biodegradable polymers, have been chosen for use as binders for HA because they are considered “green polymers” and reduce its brittleness [13–15]. Poly(vinyl pyrrolidone) is a water-based polymer, and it has been considered an eco-friendly polymer.

L. C. Mendes (✉) · R. C. Rodrigues  
Instituto de Macromoléculas Professora Eloisa Mano-IMA,  
Universidade Federal do Rio de Janeiro-UFRJ, Centro de  
Tecnologia, Bloco J, P.O. Box 68525, Avenida Horácio Macedo,  
2030, Rio de Janeiro, RJ 21941-598, Brazil  
e-mail: lcgmendes@ima.ufrj.br

E. P. Silva  
Nucleo de Pesquisa Produtos Naturais-NPPN, Universidade  
Federal do Rio de Janeiro-UFRJ, Rio de Janeiro, RJ, Brazil

Its applications comprise areas in cosmetics, construction and building cements, and as a stabilizer for metal in nanoparticle systems where it is used as a binder material [16, 17]. Besides being a water-soluble polymer, it is known as a biocompatible and non-toxic material, and is largely employed in traditional pharmaceutical formulations. It has recently shown great appeal in drug delivery compositions [18–21].

This article describes the preparation and characterization of PVP/HA composites with HA content of 20, 50 and 80 wt%. The assessment of the thermal, structural, morphological properties was carried out.

## Experimental

### Preparation of hydroxyapatite and composites

HA was synthesized according to the following procedure. The solution A (250 mL of the 0.30 M  $(\text{NH}_4)_2\text{HPO}_4$  aqueous solution, at pH 11, adjusted by addition of 12 mL de  $\text{NH}_4\text{OH}$ ) was added to solution B (250 mL of the 0.50 M  $\text{Ca}(\text{NO}_3)_2 \cdot 4\text{H}_2\text{O}$  aqueous solution, at pH 11, adjusted by addition of 10 drops of  $\text{NH}_4\text{OH}$ , with a flow rate of 100  $\text{mL h}^{-1}$ , under mechanical stirring (500 rpm), the reaction medium being maintained at 353 K, for 300 min. On completion, the reaction mixture was allowed to reach room temperature and a white solid on the flask bottom was noticed. The remaining liquid was decanted and the solid was washed with distilled water until it attained neutral pH. Finally, the solid was dried in a vacuum oven at 323 K, until reaching constant weight.

The composites PVP/HA were prepared by gradual addition of different weight percentages of HA (20, 50 and 80 wt%) into a glass flask containing 50 mL of the 0.036 M PVP ethanolic solution, under magnetic stirring, at 298 K. The suspension was poured into a rectangular mold ( $4 \times 2 \times 1$  cm) and was left overnight for solvent evaporation. Finally, the material was dried in a vacuum oven at 323 K, to eliminate the residual solvent.

### Characterization

#### X-ray fluorescence (XRF)

An X-ray microscope Rigaku, model RIX 3100 was used to determine the ratio Ca/P of the HA. The ratio between the calcium oxide and phosphorus pentoxide contents was considered.

#### Fourier transform infrared spectroscopy (FT-IR)

FT-IR spectra of the samples were obtained from KBr disk using a Varian equipment model 3100 Excalibur Series,

with resolution of  $2 \text{ cm}^{-1}$  and 40 scans, in the range of 4,000–400  $\text{cm}^{-1}$ , with the purpose of evaluating the potential interactions between PVP and HA.

#### Wide angle X-ray diffraction (WAXD)

Wide angle X-ray diffraction was performed in a Rigaku equipment model Miniflex using  $\text{Cu } K_\alpha$  radiation at 30 mA, 40 kV,  $2\theta$  scans from 2 to 50° with 0.033° of resolution, to assess the crystalline structure of the HA, solely and in the composites.

#### Differential scanning calorimetry (DSC)

Differential scanning calorimetry was carried out in a TA equipment model Q1000, at different cycles, under nitrogen atmosphere, using 5–10 mg of sample weight. The first cycle of heating was performed from 333 to 503 K, at  $283 \text{ K min}^{-1}$ , kept at 503 K for 3 min, to erase the previous thermal history. After that, the sample was submitted to a cooling process down to 333 K, at  $473 \text{ K min}^{-1}$ . Finally, the sample was reheated up to 503 K, at the same rate of the 1st scan. The registered changes on the calorimetric curves were evaluated.

#### Thermogravimetry/differential thermogravimetry (TG/DTG)

Thermal stability of the samples was estimated by thermogravimetry/differential thermogravimetry curves registered in a TA equipment model Q500, using sample weight of 5–6 mg, temperature range 303–973 K, at  $293 \text{ K min}^{-1}$ , under nitrogen atmosphere. The initial, final, and maximum degradation temperatures were described.

## Results and discussion

The chemical composition of HA from X-ray fluorescence analysis is listed in Table 1. The ratio Ca/P was 2.04 which is rather close to the theoretical value considering the chemical structure of the HA— $\text{Ca}_{10}(\text{PO}_4)_6(\text{OH})_2$ .

**Table 1** Composition of HA

Oxide	Content/%
CaO	55.50
$\text{P}_2\text{O}_5$	44.20
MgO	0.10
$\text{SiO}_2$	0.10
$\text{Al}_2\text{O}_3$	0.08

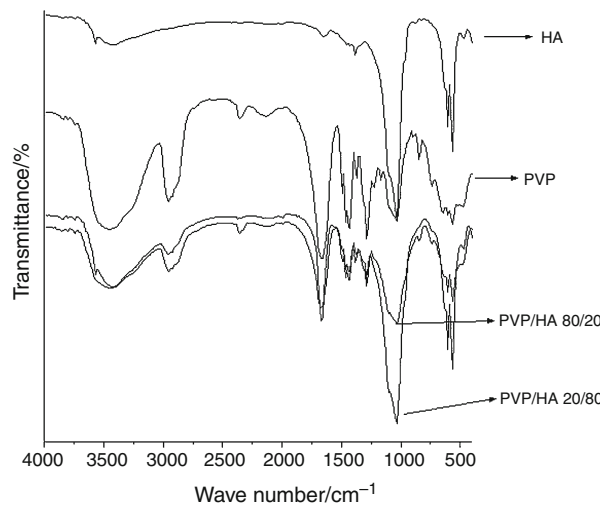


**Fig. 1** Spectra of FT-IR of HA, PVP and composites

Figure 1 shows the FT-IR spectra of the samples. Tables 2 and 3 present the main frequency, assignment, and vibration mode of the parent components. Owing to their similarities, the sample PVP/HA (20/80) was selected to show the infrared data of the composites (Table 4).

The HA spectrum shows the  $\text{PO}_4^{3-}$  absorptions at 476, 565, 603, 964, 1037, and  $1101\text{ cm}^{-1}$  attributed to the P–O bending and symmetric stretching vibrations. The peak ascribed to the hydroxyl stretching was split into two, the maxima of which are located at  $3,576$  and  $3,448\text{ cm}^{-1}$  and were regarded as being the reflections of the absorbed and combined water, respectively. At low frequency ( $638\text{ cm}^{-1}$ ), a weak peak was observed ascribed to the O–H bending vibration [22]. The weak peak at  $1,658\text{ cm}^{-1}$  merged into two types of vibrations—in-plane bending of H–O–H molecules and carbonyl stretching of the carbonate

**Table 2** FT-IR frequency, assignment, and mode of vibration of HA

Frequency/cm <sup>-1</sup>	Assignment	Vibration mode
3,576	$\text{H}_2\text{O}$ absorbed	Stretching O–H
3,448	$\text{H}_2\text{O}$ combined	Stretching O–H
1,658	$\text{CO}_3^{2-}$ , $\text{H}_2\text{O}$	Stretching C–O, bending O–H
1,463	$\text{CO}_3^{2-}$	Stretching C–O
1,425	$\text{CO}_3^{2-}$	Stretching C–O
1,386	$\text{NO}_3^-$	Stretching N–O
1,101	$\text{PO}_4^{3-}$	Stretching P–O
1,037	$\text{PO}_4^{3-}$	Stretching P–O
964	$\text{PO}_4^{3-}$	Bending P–O
877	$\text{HPO}_4^{2-}$	Bending P–O
638	$\text{H}_2\text{O}$	Bending O–H
603	$\text{PO}_4^{3-}$	Bending P–O
565	$\text{PO}_4^{3-}$	Bending P–O
476	$\text{PO}_4^{3-}$	Bending P–O

**Table 3** FT-IR frequency, assignment, and mode of vibration of PVP

Frequency/cm <sup>-1</sup>	Assignment	Vibration mode
3,466	$\text{H}_2\text{O}$ combined	Stretching O–H
2,962	$\text{CH}_2$	Stretching C–H
2,933	$\text{CH}_2$	Stretching C–H
2,904	CH	Stretching C–H
1,670	$\text{C=O}$	Stretching C–O
1,494	$\text{CH}_2$	Bending $\text{CH}_2$
1,463	$\text{CH}_2$	Bending $\text{CH}_2$
1,444	$\text{CH}_2$	Bending C–H
1,429	$\text{CH}_2$	Bending C–H
1,292	C–N	Stretching C–N
1,172	$\text{C=O}$	Axial and angular bending C–C(=O)
850	$\text{O=C–N–CH=CH}_2$	Out of plane bending $\text{CH}_2$
740	$\text{CH}_2$	Bending C–H
655	—	—
576	—	—

ion. The latter was attributed to carbon dioxide absorbed during the HA preparation. The absorptions at  $1,463$  and  $1,425\text{ cm}^{-1}$  were also associated to that ion whereas the peak assigned at  $1,386\text{ cm}^{-1}$  could be related to the residual nitrate [5, 6].

Table 3 shows the absorptions taken from PVP spectrum. The outstanding ones at  $1,670$  and  $1,172\text{ cm}^{-1}$  were considered as carbonyl stretching, symmetric, and asymmetric, respectively, whereas at  $1,292$  and  $740\text{ cm}^{-1}$  were attributed to C–N stretching and C–H bending [23].

**Table 4** FT-IR frequency, assignment, and mode of vibration of PVP/HA (20/80) composite

Frequency/cm <sup>-1</sup>	Assignment	Vibration mode
3,574	$\text{H}_2\text{O}$ absorbed	Stretching O–H
3,448	$\text{H}_2\text{O}$ combined	Stretching O–H
2,964	$\text{CH}_2$	Stretching C–H
1,665	$\text{C=O}$	Stretching C–O
1,463	$\text{CO}_3^{2-}$	Stretching C–O
1,446	$\text{CH}_2$	Bending C–H
1,427	$\text{CO}_3^{2-}$	Stretching C–O
1,386	$\text{NO}_3^-$	Stretching N–O
1,294	C–N	Stretching C–N
1,097	$\text{PO}_4^{3-}$	Stretching P–O
1,035	$\text{PO}_4^{3-}$	Stretching P–O
964	$\text{PO}_4^{3-}$	Bending P–O
740	$\text{CH}_2$	Bending C–H
636	$\text{PO}_4^{3-}$	Bending P–O
603	$\text{PO}_4^{3-}$	Bending P–O
565	$\text{PO}_4^{3-}$	Bending P–O

The main infrared absorptions of PVP and HA were noticed in the composite spectra but the peak intensities were changeable with composition (Fig. 1; Table 4). In all composites, the PVP carbonyl symmetric stretching vibration was shifted to lower frequency due to the formation of hydrogen bond with HA hydroxyl groups. The same result was found by Silva and collaborators in PVP/lignin blends [24].

The WAXD patterns, Bragg angles, and crystallographic planes of the materials are presented in Fig. 2 and Tables 5–6. The HA Bragg angles and their respective diffraction planes (Table 5) are in agreement with those reported by Morales and Siddharthan [5, 25]. The diffractogram of PVP, unexpectedly, revealed two broad peaks which  $2\theta$  are located around 12 and 22°. This result leads to the conclusion that a kind of enthalpic relaxation might have occurred producing a certain degree of order of the PVP chains. With respect to the composite WAXD data, the HA crystallographic planes sharply appeared insofar as the amount of HA increased in the composites. The peaks regarded to  $2\theta$  angles around 30–35, 39, 46, and 49° seem to increase their intensities while the new crystallographic planes—(210), (310), and (213)—came from the WAXD curve of the PVP/HA 20/80 (Fig. 2; Table 6). The enthalpic relaxation of the PVP chains seems to occur at lesser extension in the composites.

The calorimetric curves of the HA, PVP, and the composites with 50 and 80 wt% of HA are shown in Figs. 3 and 4, respectively. At the first cycle of heating (Fig. 3), the curve of HA presented a broad and very low intensity peak between 343 and 433 K which was attributed to the release of adsorbed and combined water. A similar result was reported by Siddharthan and co-workers in their study

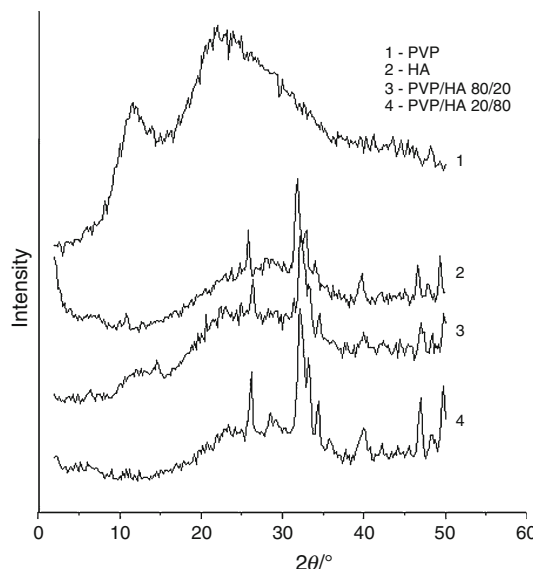


**Fig. 2** WAXD of HA, PVP, and composites

**Table 5** Bragg angles and their respective crystallographic planes for HA

Bragg angle/ $2\theta$	Crystallographic plane
25.7	(002)
31.8	(211)
32.2	(112)
33.0	(300)
34.0	(202)
39.7	(113)
46.6	(320)
49.4	(321)

**Table 6** Bragg angles and their respective crystallographic planes for composites

Composite PVP/HA	Bragg angle/ $2\theta$	Crystallographic plane
80/20	26.4	(002)
	32.2	(211)
	33.3	(300)
	34.5	(202)
	39.7	(113)
	47.0	(320)
	49.9	(321)
	26.5	(002)
	29.4	(210)
	32.3	(211)
50/50	32.9	(112)
	33.6	(300)
	34.5	(202)
	39.7	(113)
	47.2	(320)
	48.6	(213)
	49.9	(321)
	26.2	(002)
	29.1	(210)
	32.2	(211)
	32.6	(112)
	33.3	(300)
	34.4	(202)
	35.8	(310)

on preparation of HA by a broad, intense peak with a shoulder around 373 K. The peak was ascribed to the enthalpy relaxation which is a manifestation of structural relaxation in glass polymers. Kiekens and co-authors [19] reported the occurrence of enthalpy relaxation of the PVP

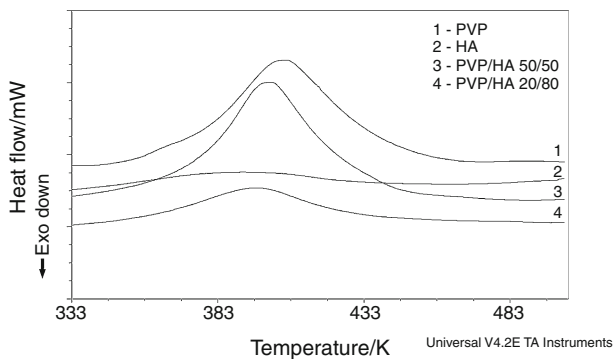


**Fig. 3** DSC curves of HA, PVP, and composites (first heating)

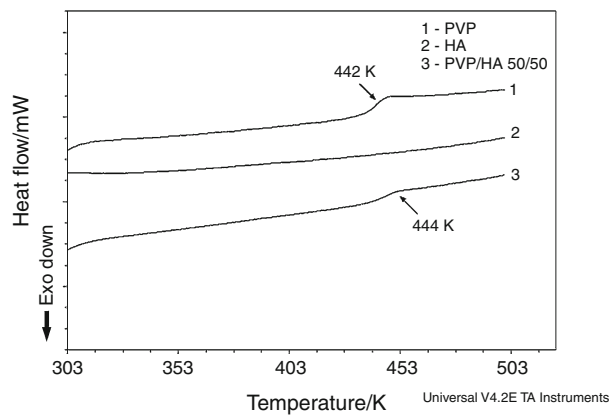


**Fig. 4** DSC curves of HA, PVP, and composites (second heating)

chains in pharmacological tablets. According to Cassu and collaborators [26], the shoulder corresponds to a PVP secondary relaxation. The composites also exhibited a peak whose intensity was reduced according to the decreased amount of PVP in the composite. Even in the presence of the HA, the enthalpic process of the PVP chains occurred in the composites. For demonstration purpose, the Fig. 4 shows the DSC curves of the second cycle of heating of the neat PVP, HA, and 50/50 PVP/HA composite. The  $T_g$  of the neat PVP was found at 442 K while that of the composite appeared at 444 K. Chrissafis et al. [27] investigated composites of poly(vinylpyrrolidone), chitosan, and poly(vinyl alcohol), and silica nanoparticles. They noticed changes on  $T_g$  of the Chi/SiO<sub>2</sub> and PVA/SiO<sub>2</sub> systems but not on the PVP/SiO<sub>2</sub> one. In the case of the two first systems, the authors considered the increase of the  $T_g$  values due to the occurrence of grafting reactions of the hydroxyl and amine groups, in the chitosan, and hydroxyl group, in the PVA, with silanol groups which are on the silica surface. Regarding the PVP/SiO<sub>2</sub> composites, they supposed that the interaction between PVP carbonyl group and hydroxyl one on the silica surface was weak. No change in PVP  $T_g$  was detected. In the case of PVP/HA composites, despite the considerable shift of the PVP carbonyl

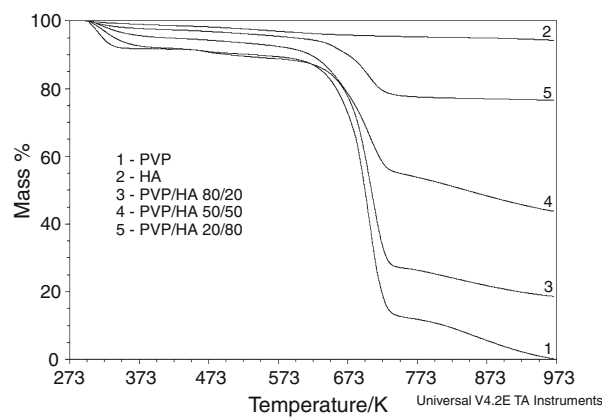


**Fig. 5** TG curves of HA, PVP, and composites

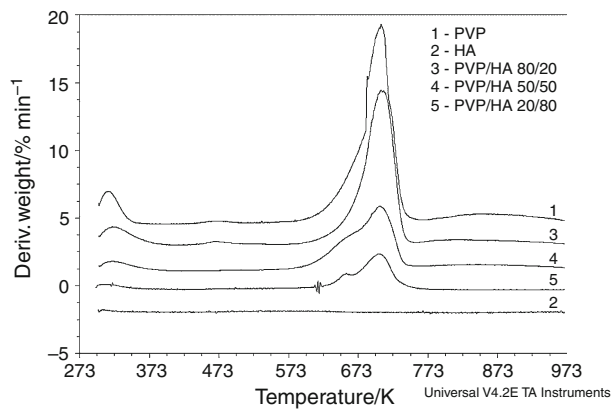


**Fig. 6** DTG curves of HA, PVP, and composites

absorption no significant change of  $T_g$  was noticed. As the  $T_g$  is essentially the same, in the composites studied herein, there is the absence of grafting and only the formation of hydrogen bond between PVP carbonyl group and water remained in the HA. This secondary bond is sufficiently strong to shift the wavenumber of the carbonyl group but will not be able to increase the  $T_g$  value. The results are in agreement with those found in the X-ray diffraction analysis.

The TG/DTG curves are shown in Figs. 5 and 6, respectively. The thermal degradation curve of the HA did not exhibit any decay whereas in the case of the PVP three decays were noticed, around 303–373, 573–773, and 773–973 K. The composite curves are between the parent components. Unexpectedly, from 573 to 773 K, the PVP derivative curve presented two maxima of which the first occurred at 685 K, while the second one was around 706 K (Figs. 6) which might be related to the release of two kinds of burning residues. The maximum at lower temperature might be attributed to the PVP pyrrolidone pendant groups and the second to the PVP hydrocarbon main chains. For the composites, there was a shift of the first maximum of

the PVP derivative curve to lower temperature related to the increased amount of HA whereas the second maximum remained almost at the same temperature (Figs. 6). Chrissafis and collaborators [28] studied mechanical properties and thermal degradation of poly( $\epsilon$ -caprolactone) (PCL) nanocomposites. They concluded that the systems with modified montmorillonite and fumed silica accelerated the thermal decomposition of the PCL due to respective aminalysis and hydrolytic reactions that the reactive groups on the surface of these materials can induce. In our study, similar to Chrissafis' results [28], the water molecules in the HA might be the reason of the accelerating effect of the PVP decomposition. Its first step of burning became sharply evidenced in the composite with high amount of HA due to hydrolytic cleavage of the pyrrolidone groups.

## Conclusions

Composites of PVP/HA were prepared to develop a material suitable for repairing bone tissue. Hydrogen bonding between the PVP carbonyl and the HA hydroxyl group was noticed. Enthalpy relaxation of PVP chains was detected which might be ascribed to the rearrangement of the PVP molecules in all materials during the solvent evaporation. The DTG curves showed that the main degradation peak of the PVP split into two in which the first one was shifted to lower temperatures as the composite was enriched by HA, and the second remained almost at the same temperature. The HA molecules seems to exert a catalytic action on PVP degradation.

## References

- Verwilghen C, Rio S, Nzihou A, Gauthier D, Flamant G, Sharrock PJ. Preparation of high specific surface area hydroxyapatite for environmental applications. *J Mater Sci*. 2007;42:6062–6.
- Santos ML, Florentino AO, Saeki MJ, Aparecida AH, Lia Fook MV, Guastaldi AC. Síntese de hidroxiapatita pelo método sol-gel utilizando precursores alternativos: nitrito de cálcio e ácido fósforico. *Eclética Química*. 2005;30:29–35.
- Ignjatovic N, Tomic S, Dakic M, Miljkovic M, Plavsic M, Uskokovic D. Synthesis and properties of hydroxyapatite/poly-L-lactide composite biomaterials. *Biomaterials*. 1999;20:809–16.
- Qiu C, Xiao X, Liu R. Biomimetic synthesis of spherical nano-hydroxyapatite in the presence of polyethylene glycol. *Ceram Int*. 2008;34:1747–51.
- Morales JG, Burgues JT, Boix T, Fraile J, Clemente RR. Precipitation of stoichiometric hydroxyapatite by a continuous method. *Cryst Res Technol*. 2001;36:15–26.
- Maachou H, Bal KE, Bal Y, Chagnes A, Cote G, Alliouche D. Characterization and in vitro bioactivity of chitosan/hydroxyapatite composite membrane prepared by freeze-gelation method. *Trends Biomater Artif Organs*. 2008;22:15–24.
- Porter AE, Patel N, Skepper JN, Best SM, Bonfield W. Comparison of in vivo dissolution processes in hydroxyapatite and silicon-substituted hydroxyapatite bioceramics. *Biomaterials*. 2003;24:4609–20.
- Landi E, Sprio S, Sandri M, Celotti G, Tamperie A. Development of Sr and CO<sub>3</sub> co-substituted hydroxyapatites for biomedical applications. *Acta Biomater*. 2008;4:656–63.
- Dumelie N, Benhayounea H, Richard D, Laurent-Maquin D, Balossier G. In vitro precipitation of electrodeposited calcium-deficient hydroxyapatite coatings on Ti6Al4V substrate. *Mater Charact*. 2008;59:129–39.
- Dalby MJ, Di Silvio L, Harper EJ, Bonfield W. Initial interaction of osteoblasts with the surface of a hydroxyapatite-poly(methylmethacrylate) cement. *Biomaterials*. 2001;22:1739–47.
- Tang XL, Xiao XF, Liu RF. Structural characterization of silicon-substituted hydroxyapatite synthesized by a hydrothermal method. *Mater Lett*. 2005;59:3841–6.
- Albano C, Cataño L, Figuera L, Perera R, Karam A, González G, Noris K. Evaluation of a composite based on high-density polyethylene filled with surface-treated hydroxyapatite. *Polym Bull*. 2009;62:45–55.
- Seong-Hoon K, Byoung-Ki L, Fangfang S, Kwangnak K, Su-Chak R, Hong-Sung K, Jaebeom L. Preparation of high flexible composite film of hydroxyapatite and chitosan. *Polym Bull*. 2009;62:111–8.
- Ignjatovic N, Savic V, Najman S, Plavsic M, Uskokovic D. A study of HAp/PLLA composite as a substitute for bone powder using FT-IR spectroscopy. *Biomaterials*. 2001;22:571–5.
- Khan YM, Katti DS, Laurencin CT. Novel polymer-synthesized ceramic composite-based system for bone repair: an in vitro evaluation. *J Biomed Mater Res*. 2004;69:728–37.
- Lee K-C, Her J-H, Kwon S-K. Red clay composites reinforced with polymeric binders. *Constr Build Mater*. 2008;22:2292–8.
- Tae-Hyun K, Dae-Wook K, Jong-Min L, Yong-Geun L, Seong-Geun O. Preparation of gold-silica heterogeneous nanocomposite particles by alcohol-reduction method. *Mater Res Bull*. 2008;43:1126–34.
- Mandal U, Gowda V, Ghosh A, Selvan S, Solomon S, Pal TK. Formulation and optimization of sustained release matrix tablet of metformin HCl 500 mg using response surface methodology. *Yakugaku Zasshi*. 2007;127:1281–90.
- Kiekens F, Zelko R, Remon JP. Effect of the storage conditions on the tensile strength of tablets in relation to the enthalpy relaxation of the binder. *Pharm Res*. 2000;17:490–3.
- Gohel MC, Jogani PD. Exploration of melt granulation technique for the development of coprocessed directly compressible adjuvant containing lactose and microcrystalline cellulose. *Pharm Dev Technol*. 2003;8:175–85.
- Kiekens F, Zelko R, Remon JP. Influence of drying temperature and granulation liquid viscosity on the inter- and intragranular drug migration in tray-dried granules and compacts. *Pharm Dev Technol*. 2000;5:131–7.
- Jevtic M, Radulovic A, Ignjatovic N, Mitric M, Uskokovic D. Controlled assembly of poly(D, L-lactide-co-glycolide)/hydroxyapatite core-shell nanospheres under ultrasonic irradiation. *Acta Biomater*. 2009;5:208–18.
- Hummel DO. Atlas of polymer and plastics analysis V.2B/I. Munich, Germany: Carl Hansen; 1988.
- Silva M, Silva FCA, Fogo FC, Pineda EAG, Hechenleitner AAW. Thermal and FTIR study of poly(vinylpyrrolidone)/lignin blends. *J Therm Anal Calorim*. 2005;79:367–70.
- Siddharthan A, Seshadri SK, Sampath SK, Kumar TS. Synthesis of calcium deficient hydroxyapatite nanoparticles by microwave irradiation. *Trends Biomater Artif Organs*. 2005;18:110–3.
- Cassu SN, Felisberti MI. Poly(vinyl alcohol) and poly(vinylpyrrolidone) blends: 2. Study of relaxations by dynamic mechanical analysis. *Polymer*. 1999;40:4845–51.

27. Chrissafis K, Paraskevopoulos KM, Papageorgiou GZ, Bikiaris DN. Thermal and dynamic mechanical behavior of bionano-composites: fumed silica nanoparticles dispersed in poly(vinyl-pyrrolidone), chitosan and poly(vinyl alcohol). *J Appl Polym Sci.* 2008;110:1739–49.
28. Chrissafis K, Antoniadis G, Paraskevopoulos KM, Vassiliou A, Bikiaris DN. Comparative study of the effect of different nanoparticles on the mechanical properties and thermal degradation mechanism of in situ prepared poly( $\epsilon$ -caprolactone) nanocomposites. *Comp Sci Technol.* 2007;67:2165–74.